doi:10.1038/nature11934

Femtosecond switching of magnetism via strongly correlated spin–charge quantum excitations

Tianqi Li[1,2], Aaron Patz[1,2], Leonidas Mouchliadis[3,4], Jiaqiang Yan[2]†, Thomas A. Lograsso[2], Ilias E. Perakis[3,4] & Jigang Wang[1,2]

The technological demand to push the gigahertz (10^9 hertz) switching speed limit of today's magnetic memory and logic devices into the terahertz (10^{12} hertz) regime underlies the entire field of spin-electronics and integrated multi-functional devices. This challenge is met by all-optical magnetic switching based on coherent spin manipulation[1]. By analogy to femtosecond chemistry and photosynthetic dynamics[2]—in which photoproducts of chemical and biochemical reactions can be influenced by creating suitable superpositions of molecular states—femtosecond-laser-excited coherence between electronic states can switch magnetic order by 'suddenly' breaking the delicate balance between competing phases of correlated materials: for example, manganites exhibiting colossal magneto-resistance suitable for applications[3,4]. Here we show femtosecond (10^{-15} seconds) photo-induced switching from antiferromagnetic to ferromagnetic ordering in $Pr_{0.7}Ca_{0.3}MnO_3$, by observing the establishment (within about 120 femtoseconds) of a huge temperature-dependent magnetization with photo-excitation threshold behaviour absent in the optical reflectivity. The development of ferromagnetic correlations during the femtosecond laser pulse reveals an initial quantum coherent regime of magnetism, distinguished from the picosecond (10^{-12} seconds) lattice-heating regime characterized by phase separation without threshold behaviour[5,6]. Our simulations reproduce the nonlinear femtosecond spin generation and underpin fast quantum spin-flip fluctuations correlated with coherent superpositions of electronic states to initiate local ferromagnetic correlations. These results merge two fields, femtosecond magnetism in metals and band insulators[1,7–9], and non-equilibrium phase transitions of strongly correlated electrons[10–17], in which local interactions exceeding the kinetic energy produce a complex balance of competing orders.

There is growing evidence that femtosecond transient polarization of condensed matter systems during a laser pulse can be used to manipulate spin or change magnetic order[1,7–9,18–20]. Non-adiabatic coherent photo-excitation during very early times can be used to control subsequent slower dynamics driven by the free energy or excited potential surface[21]. In strongly correlated materials, such as colossal magneto-resistive (CMR) manganite and high-T_c copper oxide systems, prior ultrafast spectroscopy experiments mostly concentrated on laser-induced melting of electronic charge order and orbital order (CO/OO), and on structural phase transformations[15–17]. Thus far experiments directly probing magnetism only showed picosecond and nanosecond spin generation, much slower than the femtosecond excitation pulse, without threshold dependence on laser intensity[5,6,22,23]. At such 'long timescales', lattice heating and phase separation dynamics dominate, as seen, for example, in some CMR manganites[5,6] (see also ref. 24, where it is shown that laser heating of materials with high temperature ferromagnetic orders can induce magnetization). Transient magnetism there was mostly indirectly inferred by transferring static pictures and quasi-equilibrium theories to the ultrafast regime.

Here we excite the antiferromagnetic (AFM) CO/OO ground state of CMR manganites shown in Fig. 1a, which consists of one-dimensional zig-zag chains with alternating manganese Mn^{4+}/Mn^{3+} atoms (charge order) and ferromagnetically-aligned spins. This particular antiferromagnetic structure is called CE-type AFM[3,4]. Neighbouring chains are AFM-ordered, which restricts inter-chain electron hopping because of the large magnetic energy penalty (Hund's rule). The Mn^{4+} atom t_{2g} orbitals[3,4] are occupied by three electrons forming local $S = 3/2$ spins, S_i. In the Mn^{3+} atoms, an additional electron of spin s_i populates a Mn e_g orbital[3,4]. The resulting Jahn–Teller distortion of MnO_6 octahedra lifts the e_g orbital degeneracy on the Mn^{3+} atoms, which are then populated by alternating $d_{3x^2-r^2}/d_{3y^2-r^2}$ orbitals (orbital order)[3,4]. The measured phase diagram of our $Pr_{0.7}Ca_{0.3}MnO_3$ manganite, Fig. 1b, results from the competition between these AFM CO/OO insulating and ferromagnetic metallic phases. The ground state is however always insulating under weak magnetic fields ($B < 0.5$ T in our experiment), for all relevant temperatures. It exhibits CO/OO below ~200 K and CE-type AFM below the Néel temperature, $T_N \approx 140$ K (shaded area). Thus, heating of our system cannot induce ferromagnetism, unlike those systems with high-temperature ferromagnetic orders[24].

This Letter reports a femtosecond AFM to ferromagnetic phase transition in $Pr_{0.7}Ca_{0.3}MnO_3$. In particular, we observe a threshold excitation fluence for inducing a huge magnetization during coherent nonlinear optical excitation of the CE-type AFM CO/OO ground state by a 82-fs laser pulse. To see this, we performed two-colour—near-infrared pump (1.55 eV), ultraviolet probe (3.1 eV)—femtosecond-resolved magnetic circular dichroism (MCD) and magneto-optical Kerr rotation (MOKE) measurements. This geometry allows us to observe, at 3.1 eV, genuine femtosecond spin dynamics of the t_{2g} electron magnetization component S_z perpendicular to the sample surface, induced by the pump (see Methods). We measure femtosecond changes in the complex magneto-optical angle $\tilde{\Theta}_K = \theta_k + i\eta_k$, where the imaginary part η_k (MCD) and real part θ_k (MOKE) correspond to absorption difference and phase shift, respectively, between right- and left-circularly polarized light, induced by $S_z(t)$.

Typical temporal profiles of the pump-induced ellipticity change, $\Delta\eta_k$, during the first 5 ps are shown in Fig. 1c, at 30 K and for two pump fluences. $\Delta\eta_k > 0$ indicates photo-induced magnetization from the AFM ground state. At low pump fluence, 0.64 mJ cm^{-2} (red filled circles), we only observe a gradual, picosecond magnetization rise. An increase of pump fluence to 5.8 mJ cm^{-2} (open circles) reveals a remarkable femtosecond regime of spin photogeneration: a huge quasi-instantaneous jump in magnetization, three orders of magnitude larger than in magnetic semiconductors[20,25], now precedes picosecond spin dynamics. Deconvolution of the $\Delta\eta_k$ and probe pulse temporal profiles give a fast magnetization rise time of ~120 fs (Fig. 1c, inset). The clear discontinuity of $\Delta\eta_k$ (dashed line, Fig. 1c) marks two different temporal regimes of transient magnetism. Figure 2a shows the detailed pump-fluence dependence of $\Delta\eta_k$: it reveals a photo-excitation threshold, $I_{th} \approx 2.5$ mJ cm^{-2}, for the

[1]Department of Physics and Astronomy, Iowa State University, Ames, Iowa 50011, USA. [2]Ames Laboratory – USDOE, Ames, Iowa 50011, USA. [3]Department of Physics, University of Crete, Heraklion, Crete 71003, Greece. [4]Institute of Electronic Structure and Laser, Foundation for Research and Technology-Hellas, Heraklion, Crete 71110, Greece. †Present addresses: Department of Materials Science and Engineering, University of Tennessee, Knoxville, Tennessee 37996, USA; Materials Science and Technology Division, Oak Ridge National Laboratory, Oak Ridge, Tennessee 37831, USA.

©2013 Macmillan Publishers Limited. All rights reserved

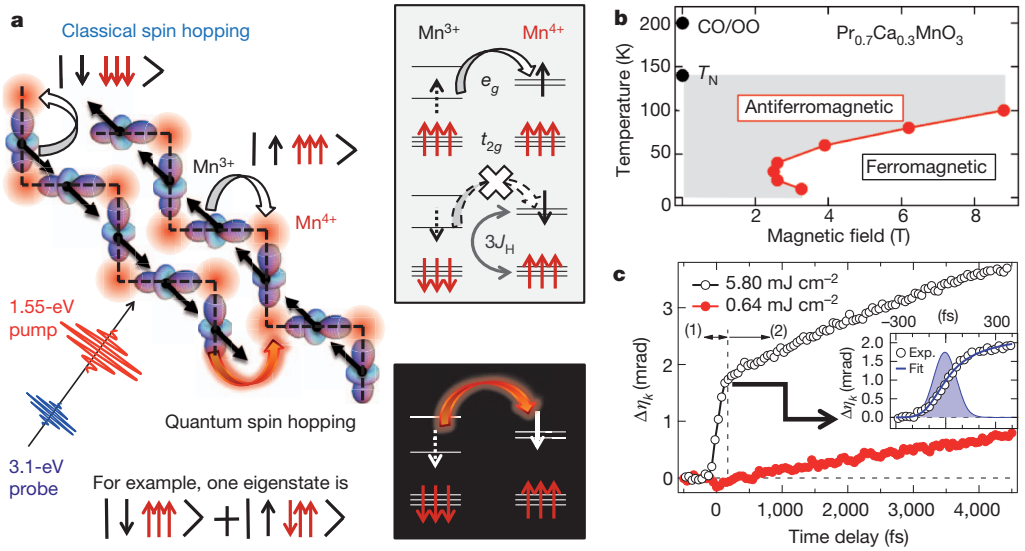

Figure 1 | A quantum many-body scheme for femtosecond switching of magnetism and ultrafast photo-induced spin dynamics in $Pr_{0.7}Ca_{0.3}MnO_3$. **a**, Schematics of ultrafast excitations of the CE-type AFM/CO/OO order, whose spin, charge, and orbital lattice pattern, shown in the left panel, consists of one-dimensional AFM-coupled zig-zag chains. For classical spins (right top panel), electron conduction and optical transitions are restricted within the same one-dimensional ferromagnetic chain because $J = S - 1/2$ total spin configurations are suppressed by Hund's rule (white arrow, classical spin hopping). Quantum spin-flip fluctuations (right bottom), however, allow e_g electrons to hop on sites with opposite local t_{2g} spin, by forming non-equilibrium total spin eigenstates (see equation (1)) as illustrated (red arrow, quantum spin hopping). **b**, The equilibrium phase diagram of our $Pr_{0.7}Ca_{0.3}MnO_3$ sample as a function of temperature and magnetic field (sweeping up). The red dots show the measured boundary between the antiferromagnetic and ferromagnetic phases. Note that, for sufficiently small magnetic fields, the antiferromagnetic insulating phase persists at all temperatures. **c**, Ultrafast photo-induced ellipticity change $\Delta\eta_k$ for magnetic field $B = 0.5$ T and temperature $T = 30$ K for low (0.64 mJ cm^{-2}, red dots) and high (5.8 mJ cm^{-2}, open circles) pump photo-excitation intensity. The femtosecond magnetism (temporal regime (1)) is clearly distinguished from the picosecond magnetism (temporal regime (2)) and only appears for high intensity. Inset, the instrument response time (shaded) and the convolution of the probe pulse with a double-exponential time-dependent magnetization increase. We extract time constants $\tau_1 = 120$ fs (fast femtosecond magnetization) and $\tau_2 = 18{,}500$ fs (slow picosecond magnetization). Open circles, experimental results (Exp); solid curve, double-exponential fit (Fit).

emergence of femtosecond magnetization. In contrast, the charge dynamics, measured by the pump-induced reflectivity change $\Delta R/R$ (Fig. 2b), exhibits no threshold, which rules out melting of the CO/OO as the main origin of I_{th}. The critical fluence dependence exclusively for the femtosecond spin dynamics represents a hallmark of non-equilibrium magnetic phase transitions.

Further evidence for femtosecond change of magnetic ordering is presented in Fig. 3a, which compares the MCD $\Delta\eta_k$ and MOKE $\Delta\theta_k$ at two pump fluences and demonstrates notable differences between femtosecond and picosecond time intervals. Both MOKE and MCD demonstrate the existence of a fluence threshold for observing a distinct femtosecond pump-induced magnetization, with the same I_{th} in both (Supplementary Information). Such coincidence corroborates our conclusions. In contrast, the picosecond components of $\Delta\eta_k$ and $\Delta\theta_k$ exhibit different temporal profiles (for example, a damped oscillation is absent in MOKE) without threshold, indicative of slow thermal non-magnetic contributions[5,6]. In Fig. 3b, the femtosecond magnetization vanishes when the magnetic field is reduced from 0.5 T to 0 T, again pointing to the magnetic origin of the 'discontinuity' in $\Delta\eta_k$ and $\Delta\theta_k$ and, thereby, the fast spin generation during the excitation pulse.

Furthermore, the observed femtosecond spin photogeneration depends sensitively on temperature and AFM order (Fig. 3c). At

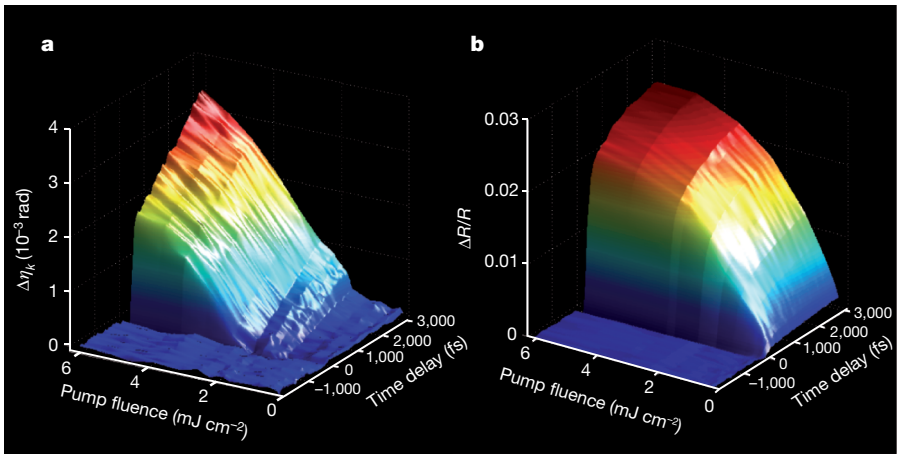

Figure 2 | A three-dimensional view demonstrating the distinct femtosecond spin and charge dynamics as well as photo-excitation threshold behaviour. **a**, Time-resolved ellipticity change $\Delta\eta_k$ and **b**, differential optical reflectivity $\Delta R/R$ as function of pump fluence. Measurements are taken under the same experimental conditions. A photo-excitation threshold $I_{th} \approx 2.5$ mJ cm^{-2} is seen for emergence of femtosecond magnetization ($\Delta\eta_k$), whereas the charge dynamics exhibits no threshold. Magnetic field $B = 0.5$ T and temperature $T = 30$ K.

©2013 Macmillan Publishers Limited. All rights reserved

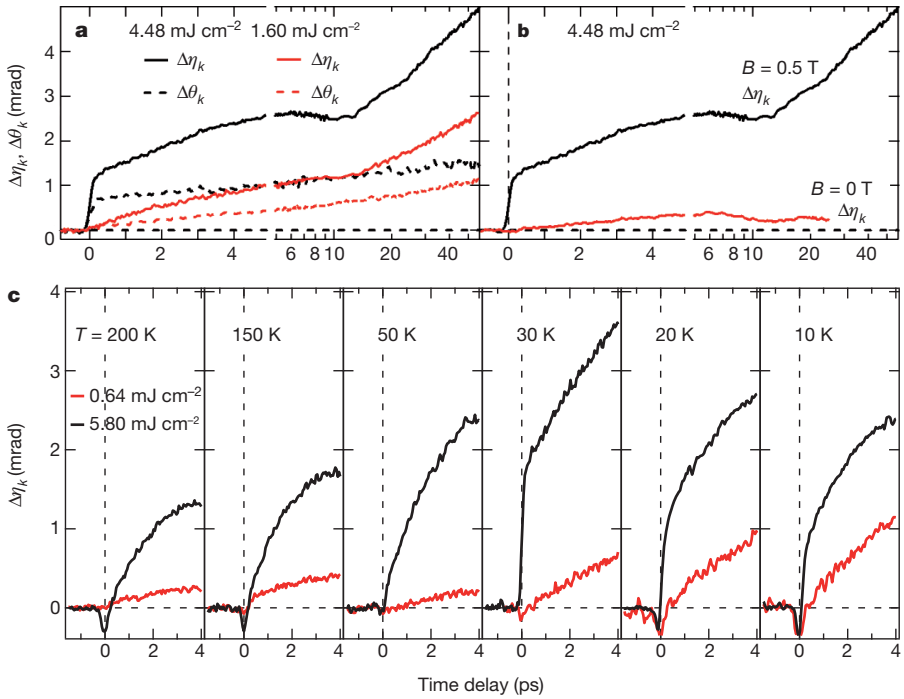

Figure 3 | Evidence for genuine femtosecond switching of magnetic ordering and its sensitive temperature dependence. **a**, Comparison between ellipticity $\Delta\eta_k$ (solid lines) and MOKE $\Delta\theta_k$ (dashed lines) under pump excitation fluences of 4.48 mJ cm^{-2} (black) and 1.60 mJ cm^{-2} (red). **b**, Magnetic field dependence of the ultrafast photo-induced ellipticity change during the first 5 ps (split axis) and for extended time intervals up to 60 ps (logarithmic scale). Black, $B = 0.5$ T; red, $B = 0$ T. $T = 30$ K. **c**, Temperature dependence of the photo-induced ellipticity for the first 4 ps under two pump excitation fluences of 0.64 mJ cm^{-2} (red) and 5.80 mJ cm^{-2} (black). Note the non-monotonic dependence of the femtosecond photo-induced magnetization on temperature: it peaks at around 30 K.

200 K and 150 K, that is, above the AFM phase transition, we observe negligible femtosecond magnetization components for all fluences used. The femtosecond magnetization appears at 50 K above threshold, reaches its maximum around 30 K, and then decreases again at lower temperatures of 20 K and 10 K. We attribute this behaviour to the competition between spin stiffness—describing the rigidity of the AFM order—and thermal fluctuations, which display opposite temperature dependence. We note that the measured temperature for maximum femtosecond spin generation, 30 K, corresponds to the minimum critical B field required for driving an AFM to ferromagnetic phase transition in Fig. 1b.

Figure 4a and b compares the pump-fluence dependence of $\Delta\eta_k$ and $\Delta R/R$ at two fixed times for the data shown in Fig. 2a and b, $\Delta\tau = 200$ fs and 6 ps: we make two observations. First, any threshold dependence of photo-induced magnetization clearly smears out in the picosecond $\Delta\eta_k$ data (black open circles), which shows a linear power dependence, and is absent in both picosecond (red open circles) and femtosecond (filled red squares) $\Delta R/R$. Thresholdless behaviours can be attributed to phonon-assisted phase separation[5,6]. However, the distinct nonlinear pump fluence and threshold dependence of the femtosecond spin dynamics (Fig. 4a) reveal a new femtosecond magnetism nonthermal temporal regime during coherent nonlinear photo-excitation, well-distinguished from the picosecond thermal temporal regime. Second, the femtosecond build-up of ferromagnetic correlations above threshold I_{th} coincides with a transition, at I_{NL}, from linear to nonlinear intensity dependence of $\Delta R/R$ (shaded area). Such coincidence suggests that global electronic conducting paths emerging from photo-induced interchain hopping are important for femtosecond (but not picosecond) magnetism.

Can we attribute our observation of femtosecond magnetism to the photodoping of the AFM ground state with electrons and holes? A transition from AFM to ferromagnetic states with electron doping was predicted for Hamiltonians without CO/OO[26], but these states are unstable to phase separation: ferromagnetic polarons, that is, an electron surrounded by a ferromagnetically aligned neighbouring spin 'cluster', form locally inside the AFM matrix[26]. Above critical doping, polaron percolation results in a global ferromagnetic ground state. At equilibrium, electron doping of the CE/CO/OO state (Fig. 1a, $x = ½ + \Delta x$) gives an unconventional ferromagnetic metal ($x < 1/2$), whereas the system remains CE-AFM insulating with hole doping ($x > 1/2$). Such electron–hole asymmetry, important for photodoping effects, arises from competition between electron delocalization (by canting antiparallel t_{2g} spins) and self-trapping (by Jahn–Teller distortions)[27]. However, the latter lattice processes are slow (picosecond)[23]. During femtosecond times shorter than the Jahn–Teller phonon period and thermalization times, magnetization can only be induced by fast spin-flip/canting non-equilibrium processes.

Below, we propose a non-equilibrium spin-exchange mechanism that produces ferromagnetic correlations during the femtosecond laser pulse. Classical spin scenarios[3,23] neglect spin-flips, and so electron hopping from atom to atom diminishes with increasing angle between the local spins[3]. Consequently, interchain e_g-electron hopping is suppressed by AFM spin alignment, resulting in electronic confinement within one-dimensional chains (Fig. 1a, white arrows). This, however, suppresses any femtosecond spin dynamics, as the e_g and t_{2g} spins remain parallel within the same chain[23]. We must thus turn to quantum spin scenarios and, additionally, engage the transient coherence, correlation and nonlinearity that dominate during the laser coherent excitation, a new paradigm in ultrafast magnetism. Quantum spin-flips (Fig. 1a, red arrows) allow for electron hopping to a site with antiparallel local spin, as we can now populate the degenerate non-equilibrium quantum states of photo-excited and local electron spins shown schematically in Fig. 1a, which diagonalize the strong Hund's rule interaction:

$$|i\alpha M\rangle = \sqrt{\frac{S+M+\frac{1}{2}}{2S+1}}\, c^{\dagger}_{ia\uparrow}\left|iS,M-\frac{1}{2}\right\rangle + \sqrt{\frac{S-M+\frac{1}{2}}{2S+1}}\, c^{\dagger}_{i\alpha\downarrow}\left|iS,M+\frac{1}{2}\right\rangle \quad (1)$$

©2013 Macmillan Publishers Limited. All rights reserved

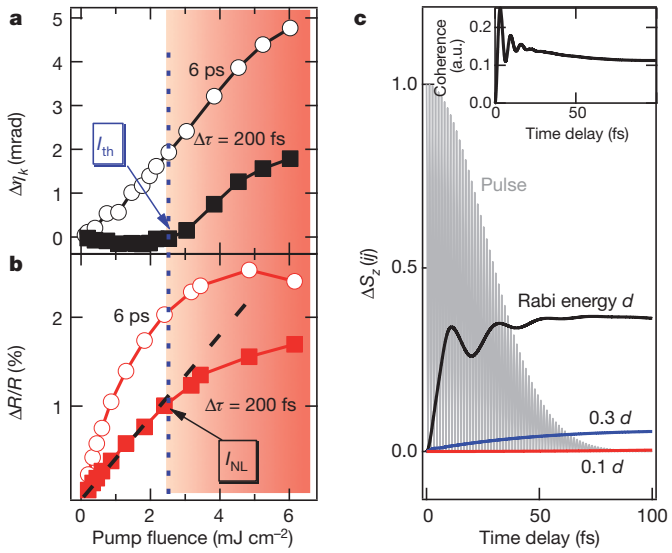

Figure 4 | Interchain femtosecond quantum spin-flip fluctuations establish ferromagnetic correlations during the coherent laser photo-excitation. **a**, Pump fluence dependence of photo-induced $\Delta\eta_K$ and **b**, $\Delta R/R$, after two time intervals, $\Delta\tau = 200$ fs (filled squares) and $\Delta\tau = 6$ ps (open circles), following photo-excitation, at 30 K. These summarize the data presented in Fig. 2a and b. The nonlinear fluence dependence with threshold I_{th} marked by the vertical dashed blue line is only seen for the femtosecond $\Delta\eta_K$. Note the different behaviour between the red shaded area (high intensity revealing femtosecond magnetism) and the low intensity regime (only picosecond magnetism). Although the photo-induced optical reflectivity change does not display any threshold behaviour, the high intensity red shaded regime above I_{NL} demonstrates a saturation nonlinear behaviour, while for low intensities below I_{NL} we observe the linear dependence on photo-excitation intensity expected from the usual perturbation expansion in terms of the optical field. **c**, Calculated photo-induced total spin for three Rabi energy values similar to those in the experiment, $d = 70$ meV (black), $0.3d$ (blue), $0.1d$(red), and inter–atomic coherence (inset) for $d = 70$ meV. The laser pulse time-dependence is superimposed (grey; $E^2(t)$), demonstrating that ferromagnetic local correlations transiently build-up from the AFM ground state (total spin zero) during the photo-excitation, with nonlinear dependence on Rabi energy and hence intensity. The time-dependence of the interatomic coherence describes 'photo-induced bond' order, which implies strong transient coupling between neighbouring atoms during the lifetime of the non-thermal populations, that is, before the establishment of a quasi-equilibrium hot temperature. The damped oscillations in the photo-induced spin, with period determined by the Jahn–Teller energy, reflect deviations from adiabaticity.

where $|iSS_z\rangle$ are the Mn^{4+} t_{2g}-spin eigenstates. The eigenvalues of the total spin $J_i = s_i + S_i$ are $J = S + 1/2$ and $M = -J, \cdots, J$. $c^{\dagger}_{i\alpha\sigma}$ adds a spin-σ electron in orbital α at site i. The quantum-coherent superposition given in equation (1), suppressed in the classical spin limit $S \rightarrow \infty$, allows for ultrafast quantum spin dynamics, driven by the off-diagonal Hund's rule magnetic interaction $J_H S_i^{\pm} \cdot s_i^{\mp}$.

In the insulating AFM state, we expect localized photo-excitations[26]. We thus describe the spin, charge and orbital populations at the ith atom by the diagonal density matrix elements $\rho_i(m) = \langle |iSm\rangle\langle iSm|\rangle$ (Mn^{4+}) and $\rho_i(\alpha M) = \langle |i\alpha M\rangle\langle i\alpha M|\rangle$ (Mn^{3+}). The 3.1-eV magneto-optical signal probes the t_{2g} spin[28] $S_z(i) = \sum_m S \cos\theta_m \rho_i(m) + \sum_{\alpha M} S \cos\theta_M \rho_i(\alpha M)$, where $\cos\theta_m = m/S$ and $\cos\theta_M = M/J$. The 1.55-eV femtosecond pump field, tuned across the Jahn–Teller insulator gap, drives coherent electron hopping between neighbouring atoms i and j with different Jahn–Teller distortions. Such quantum kinetics is hidden in static measurements[29], and the equations of motion couple $\rho_i(m)$ and $\rho_i(\alpha M)$ to the off-diagonal density matrix $\left\langle \hat{e}^{\dagger}_{\alpha'\sigma}(jM')\hat{e}_{\alpha\sigma}(iM)\right\rangle$ describing time-dependent electron–hole superpositions of electronic quantum states given by equation (1) in two different atoms i and j (bond orders). The composite fermions created by $\hat{e}^{\dagger}_{\alpha\sigma}(iM) = |i\alpha M\rangle\left\langle iS, M - \frac{\sigma}{2}\right|$ treat the strong correlation (see Supplementary Information)[30].

The solution of our density matrix equations for a two-site interchain cluster with ground state $M = S + 1/2$ (Jahn–Teller-distorted site i) and $m = -S$ (empty site j) numerically demonstrates the development of ferromagnetic correlations with femtosecond time-dependence and nonlinear dependence on photo-excitation similar to Fig. 1c, the key features of the femtosecond quantum spin regime. The calculated photo-induced spin $\Delta S_z(ij) = \Delta S_z(i) + \Delta S_z(j)$ is shown in Fig. 4c for three Rabi energies, together with the laser pulse (here the Rabi energy is $d = eEa$, where E is the optical field, e is the electron charge, and a is the lattice spacing). The decrease in Rabi energy, from $d = 70$ meV (black) to $0.1d$ (red trace), diminishes the femtosecond spin dynamics as the perturbative regime is recovered for small d. Ferromagnetic correlation, $\Delta S_z(ij) > 0$, develops during laser excitation, driven by nonlinear photo-excited interatomic coherences $\Delta\left\langle \hat{e}^{\dagger}_{\alpha'\sigma}(jM')\hat{e}_{\alpha\sigma}(iM)\right\rangle$ (see inset, Fig. 4c for $d = 70$ meV) and electron–hole asymmetry. This spin correlation is enhanced by fast virtual electron hopping due to non-thermal/coherent nonlinear population changes and photo-induced bonding. The hole, created at Mn^{3+} site i populated by parallel e_g and t_{2g} spins, leaves the t_{2g} spin unchanged. The electron is created at the neighbouring Mn^{4+} site j populated by t_{2g} spin $S_z = S$ (intrachain excitation) or $S_z = -S$ (interchain excitation). It populates a Mn^{3+} quantum state of the form given by equation (1) with $M = S_z + \sigma/2$ after interacting with the local spin. Interchain electron–hole excitations increase the $S_z = -S$ spin via spin-flip (equation (1)), thus inducing ferromagnetic correlations between AFM-aligned chains. Intrachain excitations move the $S + 1/2$ total spin along the chain and thus only affect $\Delta R/R$ and the charge distribution. The collective behaviour of these photo-induced ferromagnetic 'defects' is affected by a small magnetic field, which creates a preferred direction through spin canting[27], resulting in non-zero collective spin and enhanced interchain hopping. Such a B-field can also facilitate percolation of the photo-induced magnetic clusters, establishing macroscopic ferromagnetic order above a critical I_{th} as the local ferromagnetic cluster size grows nonlinearly. Our predicted femtosecond quantum spin canting/flip also gives rise to interchain conductive paths, which may explain I_{NL} in the femtosecond-resolved $\Delta R/R$ (Fig. 4b).

METHODS SUMMARY

Sample growth and characterization. Single crystals of $Pr_{0.7}Ca_{0.3}MnO_3$ were grown by the floating-zone method in flowing oxygen with a growth rate of 3 mm h^{-1}. X-ray powder diffraction on pulverized single crystals confirmed the single phase. The phase diagram in Fig. 1b was constructed by measuring the temperature- and field-dependence of magnetic susceptibility and electrical resistivity of our samples. Strong magnetic fields melt the AFM/CO/OO insulator ground state and induce a transition to a ferromagnetic metallic state, for example, at a critical magnetic field of $B = 5$ T at $T \approx 75$ K. This cannot be accessed by heating the sample. For our ultrafast measurements, we placed the sample in a weak magnetic field of no more than 0.5 T, pointing perpendicular to the sample surface.

Ultrafast magneto-optical spectroscopy. A Ti:sapphire amplifier with centre wavelength of 800 nm (1.55 eV), pulse duration of 82 fs at the sample position, and 1 kHz repetition rate was separated into pump and probe beams. The probe was frequency-doubled to 400 nm (3.1 eV). This photon energy produces a large magneto-optical activity due to optical transitions between oxygen $2p$ and Mn t_{2g} states[28], and thereby mostly measures dynamics of t_{2g} local spins. The probe beam was kept nearly perpendicular to the sample surface (polar MOKE geometry) ($\sim 7°$ from the normal). To a first approximation, the magneto-optical signal is proportional to $k \cdot S$, where k is the vector of the probe light. Thus, the signal measured reflects the out-of-plane magnetization component S_z of t_{2g} local spins. Our pump beam is linearly polarized, with a tunable excitation fluence of up to ~ 6 mJ cm^{-2}. There is no obvious pump polarization dependence. This two-colour pump–probe geometry was shown to maximize the magneto-optical response while minimizing the contamination of magneto-optical signals during femtosecond timescales, for example, by dichroic bleaching, spectral weight transfer associated with the electronic phase transitions, and so on. More information on data analysis and theoretical modelling that solves the time-dependent equations of motion using the Runge-Kutta routines is given in Supplementary Information.

©2013 Macmillan Publishers Limited. All rights reserved

Received 25 September 2012; accepted 21 January 2013.

1. Bigot, J. Y., Vomir, M. & Beaurepaire, E. Coherent ultrafast magnetism induced by femtosecond laser pulses. *Nature Phys.* **5,** 515–520 (2009).
2. Brumer, P. & Shapiro, M. Controlling chemical reactions in the quantum regime. *Phys. Today* **64,** 11 (2011).
3. Dagotto, E., Hotta, T. & Moreo, A. Colossal magnetoresistant materials: the key role of phase separation. *Phys. Rep.* **344,** 1–153 (2001).
4. Tokura, Y. & Nagaosa, N. Orbital physics in transition-metal oxides. *Science* **288,** 462–468 (2000).
5. McGill, S. A. *et al.* Optical evidence for transient photoinduced magnetization in $La_{0.7}Ca_{0.3}MnO_3$. *Phys. Rev. B* **71,** 075117 (2005).
6. Mertelj, T., Mamin, R., Yusupov, R. & Mihailovic, D. Ultrafast phase separation dynamics in $La_{0.875}Sr_{0.125}MnO_3$ single crystals. *Phys. Rev. B* **83,** 113103 (2011).
7. Kirilyuk, A. V. *et al.* Ultrafast optical manipulation of magnetic order. *Rev. Mod. Phys.* **82,** 2731–2784 (2010).
8. Boeglin, C. *et al.* Distinguishing the ultrafast dynamics of spin and orbital moments in solids. *Nature* **465,** 458–461 (2010).
9. Kimel, A. V. *et al.* Ultrafast non-thermal control of magnetization by instantaneous photomagnetic pulses. *Nature* **435,** 655–657 (2005).
10. Liu, M. *et al.* Terahertz-field-induced insulator-to-metal transition in vanadium dioxide metamaterial. *Nature* **487,** 345–348 (2012).
11. Fiebig, M. *et al.* Sub-picosecond photo-induced melting of a charge-ordered state in a perovskite manganite. *Appl. Phys. B* **71,** 211–215 (2000).
12. Schmitt, F. *et al.* Transient electronic structure and melting of a charge density wave in $TbTe_3$. *Science* **321,** 1649–1652 (2008).
13. Fausti, D. *et al.* Light-induced superconductivity in a stripe-ordered cuprate. *Science* **331,** 189–191 (2011).
14. Kim, K. W. *et al.* Ultrafast transient generation of spin-density-wave order in the normal state of $BaFe_2As_2$ driven by coherent lattice vibrations. *Nature Mater.* **11,** 497–501 (2012).
15. Gedik, N., Yang, D., Logvenov, G., Bozovic, I. & Zewail, A. H. Nonequilibrium phase transitions in cuprates observed by ultrafast electron crystallography. *Science* **316,** 425–429 (2007).
16. Rini, M. *et al.* Control of the electronic phase of a manganite by mode-selective vibrational excitation. *Nature* **449,** 72–74 (2007).
17. Ichikawa, H. *et al.* Transient photoinduced hidden phase in a manganite. *Nature Mater.* **10,** 101–105 (2011).
18. Zhang, G. P. *et al.* Paradigm of the time-resolved magneto-optical Kerr effect for femtosecond magnetism. *Nature Phys.* **5,** 499–502 (2009).
19. Kapetanakis, M. D., Perakis, I. E., Wickey, K. J., Piermarocchi, C. & Wang, J. Femtosecond coherent control of spins in (Ga,Mn)As ferromagnetic semiconductors using light. *Phys. Rev. Lett.* **103,** 047404 (2009).
20. Wang, J. *et al.* Memory effects in photoinduced femtosecond magnetization rotation in ferromagnetic GaMnAs. *Appl. Phys. Lett.* **94,** 021101 (2009).
21. Kapetanakis, M. D., Lingos, P. C., Piermarocchi, C., Wang, J. & Perakis, I. E. All-optical four-state magnetization reversal in (Ga,Mn)As ferromagnetic semiconductors. *Appl. Phys. Lett.* **99,** 091111 (2011).
22. Matsubara, M. *et al.* Ultrafast photoinduced insulator-ferromagnet transition in the perovskite manganite $Gd_{0.55}Sr_{0.45}MnO_3$. *Phys. Rev. Lett.* **99,** 207401 (2007).
23. Ehrke, H. *et al.* Photoinduced melting of antiferromagnetic order in $La_{0.5}Sr_{1.5}MnO_4$ measured using ultrafast resonant soft X-ray diffraction. *Phys. Rev. Lett.* **106,** 217401 (2011).
24. Miyasaka, K. *et al.* Ultrafast photoinduced magnetic moments in a charge-orbital-ordered antiferromagnetic $Nd_{0.5}Sr_{0.5}MnO_3$ thin film. *Phys. Rev. B* **74,** 012401 (2006).
25. Wang, J. *et al.* Ultrafast enhancement of ferromagnetism via photoexcited holes in GaMnAs. *Phys. Rev. Lett.* **98,** 217401 (2007).
26. Kagan, M. Y., Khomskii, D. I. & Mostovoy, M. V. Double-exchange model: phase separation versus canted spins. *Eur. Phys. J. B* **12,** 217–223 (1999).
27. Cépas, O., Krishnamurthy, H. R. & Ramakrishnan, T. V. Instabilities and insulator-metal transitions in half-doped manganites induced by magnetic-field and doping. *Phys. Rev. B* **73,** 035218 (2006).
28. Yamaguchi, S., Okimoto, Y., Ishibashi, K. & Tokura, Y. Magneto-optical Kerr effects in perovskite-type transition-metal oxides: $La_{1-x}Sr_xMnO_3$ and $La_{1-x}Sr_xCoO_3$. *Phys. Rev. B* **58,** 6862–6870 (1998).
29. Axt, V. M. & Mukamel, S. Nonlinear optics of semiconductor and molecular nanostructures; a common perspective. *Rev. Mod. Phys.* **70,** 145–174 (1998).
30. Karadimitriou, M. E., Kavousanaki, E. G., Dani, K. M., Fromer, N. A. & Perakis, I. E. Strong electronic correlation effects in coherent multidimensional nonlinear optical spectroscopy. *J. Phys. Chem. B* **115,** 5634–5647 (2011).

Supplementary Information is available in the online version of the paper.

Acknowledgements This work was supported by the National Science Foundation (contract no. DMR-1055352). Material synthesis at the Ames Laboratory was supported by the US Department of Energy-Basic Energy Sciences (contract no. DE-AC02-7CH11358). L.M. acknowledges FP7-REGPOT-2008-1, Project BIOSOLENUTI no. 229927 for financial support. L.M. and I.E.P. were partially supported by the EU Social Fund and National resources through the THALES program NANOPHOS.

Author Contributions T.L., A.P. and J.W. performed the experimental measurements, collected the data and analysed the results. L.M. and I.E.P. developed the theory and performed the time-dependent and band-structure calculations. J.Y. and T.A.L. grew the samples and characterized the single crystals. J.W. and I.E.P. designed the experiment and wrote the paper, with help from all authors.

Author Information Reprints and permissions information is available at www.nature.com/reprints. The authors declare no competing financial interests. Readers are welcome to comment on the online version of the paper. Correspondence and requests for materials should be addressed to J.W. (jgwang@iastate.edu) and I.E.P. (ilias@physics.uoc.gr).

©2013 Macmillan Publishers Limited. All rights reserved